Biochem. J. (2013) **452**, 575–584 (Printed in Great Britain) doi:10.1042/BJ20130251

online data multimedia

Formation of a tyrosine adduct involved in lignin degradation by *Trametopsis cervina* lignin peroxidase: a novel peroxidase activation mechanism

Yuta MIKI*[1], Rebecca POGNI†, Sandra ACEBES‡, Fátima LUCAS‡, Elena FERNÁNDEZ-FUEYO*, Maria Camilla BARATTO†, María I. FERNÁNDEZ*, Vivian DE LOS RÍOS*, Francisco J. RUIZ-DUEÑAS*, Adalgisa SINICROPI†, Riccardo BASOSI†, Kenneth E. HAMMEL§, Victor GUALLAR‡‖ and Angel T. MARTÍNEZ*[2]

*Centro de Investigaciones Biológicas, CSIC, Ramiro de Maeztu 9, E-28040 Madrid, Spain, †Department of Biotechnologies, Chemistry and Pharmacy, University of Siena, I-53100 Siena, Italy, ‡Joint BSC-IRB Research Program in Computational Biology, Barcelona Supercomputing Center, Jordi Girona 29, E-08034 Barcelona, Spain, §USDA Forest Service, Forest Products Laboratory, One Gifford Pinchot Drive, Madison, WI 53726, U.S.A., and ‖Institució Catalana de Recerca i Estudis Avançats (ICREA), Passeig Lluís Companys 23, E-08010 Barcelona, Spain

LiP (lignin peroxidase) from *Trametopsis cervina* has an exposed catalytic tyrosine residue (Tyr^{181}) instead of the tryptophan conserved in other lignin-degrading peroxidases. Pristine LiP showed a lag period in VA (veratryl alcohol) oxidation. However, VA-LiP (LiP after treatment with H_2O_2 and VA) lacked this lag, and H_2O_2-LiP (H_2O_2-treated LiP) was inactive. MS analyses revealed that VA-LiP includes one VA molecule covalently bound to the side chain of Tyr^{181}, whereas H_2O_2-LiP contains a hydroxylated Tyr^{181}. No adduct is formed in the Y171N variant. Molecular docking showed that VA binding is favoured by sandwich π stacking with Tyr^{181} and Phe^{89}. EPR spectroscopy after peroxide activation of the pre-treated LiPs showed protein radicals other than the tyrosine radical found in pristine LiP, which were assigned to a tyrosine–VA adduct radical in VA-LiP and a dihydroxyphenyalanine radical in H_2O_2-LiP. Both radicals are able to oxidize large low-redox-potential substrates, but H_2O_2-LiP is unable to oxidize high-redox-potential substrates. Transient-state kinetics showed that the tyrosine–VA adduct strongly promotes (>100-fold) substrate oxidation by compound II, the rate-limiting step in catalysis. The novel activation mechanism is involved in ligninolysis, as demonstrated using lignin model substrates. The present paper is the first report on autocatalytic modification, resulting in functional alteration, among class II peroxidases.

Key words: EPR, lignin model compound, lignin peroxidase (LiP), molecular docking, MS, quantum mechanics/molecular mechanics (QM/MM), tyrosine adduct.

INTRODUCTION

LiP (lignin peroxidase; EC 1.11.1.14) and VP (versatile peroxidase; EC 1.11.1.16) are haem peroxidases classified in class II of the plant/fungal/bacterial peroxidase superfamily [1]. LiP and VP are enzymes of biotechnological interest [2] owing to their high redox potential and ability to oxidize large molecules [3]. These two properties provide the ability to oxidize lignin, the recalcitrant polymer in wood and other lignocellulosic materials, as well as other high/redox/potential substrates. The latter include VA (veratryl alcohol), which is synthesized by various white-rot (lignin-degrading) basidiomycetes together with other aryl alcohols [4], and is a physiological substrate of LiP [5]. Detailed structure–function studies have shown that LiP and VP oxidize VA and other high-redox-potential substrates at a catalytic tryptophan site exposed to solvent (Trp^{171} of *Phanerochaete chrysosporium* LiP and Trp^{164} of *Pleurotus eryngii* VP), where a tryptophanyl radical is formed in the peroxide-activated enzyme via long-range electron transfer to haem [6–9]. VA is not just a substrate of LiP, but also enhances its activity towards lignin and other substrates [10]. In this context, EPR studies have demonstrated that the VA cation radical is stabilized in the presence of LiP, suggesting that it could act as a radical mediator while fixed on the enzyme surface by electrostatic forces [11,12]. Moreover, spectroscopic and kinetic studies have shown that VA can convert the inactive LiP compound III formed by excess H_2O_2 back into the resting state, suggesting that it could also protect LiP against inactivation [13].

In a previous paper, a new type of LiP was reported in the white-rot basidiomycete *Trametes cervina* [14], the type species of the new genus *Trametopsis* [15]. Chemical modification [16] and directed mutagenesis in combination with crystallographic and spectroscopic studies [17] showed that oxidation of bulky (such as ferrocytochrome *c*) and high-redox-potential (such as VA and 1,4-dimethoxybenzene) substrates by this peroxidase involves a solvent-exposed tyrosyl radical at Tyr^{181}. On the other hand, it has also been observed that pristine *T. cervina* LiP expressed in *Escherichia coli* cells, i.e. enzyme that has never been in contact with substrates, shows an unexpected initial lag period in VA oxidation, whereas the LiP recovered after several turnovers forms veratraldehyde without any lag [18]. This lag apparently indicates a self-catalytic modification that results in enzyme activation,

Abbreviations used: CID, collision-induced dissociation; DFT, density functional theory; DHP, dehydrogenation polymer; H_2O_2-LiP, lignin peroxidase after treatment with H_2O_2 alone; HCD, high-energy CID; k^{app}, apparent second-order rate constant; k_{cat}, catalytic constant; K_d, dissociation constant; K_m, Michaelis constant; k_{obs}, pseudo-first-order rate constant; LiP, lignin peroxidase; MALDI–TOF-MS, matrix-assisted laser desorption ionization–time-of-flight MS; MD, molecular dynamics; MM, molecular mechanics; MS/MS, tandem MS; nLC, nanoflow liquid chromatography; OPLS, optimized potential for liquid simulations; PMF, peptide mass fingerprinting; QM, quantum mechanics; VA, veratryl alcohol; VA-LiP, LiP after treatment with H_2O_2 and VA; VP, versatile peroxidase.

[1] Present address: Toyama Prefectural University, 5180 Kurokawa, Imizu, Toyama 939–0398, Japan.
[2] To whom correspondence should be addressed (email ATMartinez@cib.csic.es).

which has never been reported before in ligninolytic peroxidases. In the present study, we investigated this activation mechanism by comparing *T. cervina* VA-LiP (LiP after treatment with VA and H_2O_2), H_2O_2-LiP (LiP after treatment with H_2O_2 alone) and pristine LiP (with no pre-treatment). We have used MS, EPR, directed mutagenesis and stopped-flow techniques, in conjunction with molecular docking, MD (molecular dynamics) and QM (quantum mechanics)/MM (molecular mechanics) computational simulations. In addition, we have assessed the activity of VA-LiP on model lignin compounds to determine whether it is a fully functional ligninolytic peroxidase due to formation of the described adduct.

MATERIALS AND METHODS

Preparation of recombinant LiP and pre-treated VA-LiP and H_2O_2-LiP

Native (wild-type) *T. cervina* LiP (GenBank® accession number AB191466) and its Y181N variant [17] were expressed in *E. coli* cells and refolded *in vitro*, including structural Ca^{2+} and haem incorporation, as described previously [18]. For VA-LiP preparation, 10 μM LiP was incubated for 1 h at 25 °C in sodium succinate (pH 4.5) containing 10 mM VA and 0.5 mM H_2O_2. H_2O_2-LiP was prepared in the same buffer containing 0.2 mM H_2O_2. The reaction mixtures were centrifuged (26 890 ***g***, 15 min), and excess substrates and products were removed on a Superdex 75 column (using a buffer containing 1 mM $CaCl_2$ and 50 mM NaCl). The enzyme concentration was calculated using $\varepsilon_{407} = 147$ $mM^{-1} \cdot cm^{-1}$ [18].

MS analyses

Molecular masses of (pristine and pre-treated) LiP proteins were analysed by MALDI–TOF-MS (matrix-assisted laser desorption ionization–time-of-flight MS) using an Autoflex III instrument and 2,5-dihydroxyacetophenone matrix. For PMF (peptide mass fingerprinting) and MS/MS (tandem MS) analysis, the pristine and pre-treated LiP proteins were digested with Glu-C [also known as staphylococcal (*Staphylococcus aureus*) V8 protease] and analysed using a α-cyano-4-hydroxycinnamic acid matrix. The peptide mixtures from Glu-C digestion were also analysed by online nLC-MS/MS (nanoflow liquid chromatography MS/MS) on an EASY-nLC system connected to the LTQ Orbitrap Velos instrument. The peptides were separated in a BIOSPHERE C18 column (2–95 % acetonitrile in 0.1 % formic acid gradient) and directly electrosprayed into the LTQ instrument operated in data-dependent mode. Both CID (collision-induced dissociation) and HCD (high-energy CID) analyses were performed. Raw files were searched against an in-house database, and identification of modification sites was confirmed through manual inspection of the peptide spectra. See Supplementary Online Data (at http://www.biochemj.org/bj/452/bj4520575add.htm) for details of the above MS analyses.

Kinetic studies (VA oxidation)

Steady-state kinetic constants for VA oxidation were estimated from veratraldehyde formation (25 °C and pH 3.5) and K_m (Michaelis constant) and k_{cat} (catalytic constant) values were obtained. Transient-state kinetics was studied using a Bio-Logic stopped-flow device. Compound I formation was followed-up at 399 nm after mixing the resting enzyme with different H_2O_2 concentrations. Compound II formation was followed-up at 416 nm after mixing compound I (obtained by resting enzyme incubation with 1 equiv. H_2O_2) with VA. Compound II reduction was followed-up at 407 nm after mixing compound II (obtained by resting enzyme incubation with 1 equiv. H_2O_2 and 1 equiv. sodium ferrocyanide) with VA. The transient-state reactions (25 °C and pH 3.5) exhibited single exponential kinetic traces giving the k_{obs} (pseudo-first-order rate constant). When the k_{obs} showed a linear dependence of the substrate concentration, the k^{app} (apparent second-order rate constant) was obtained. When the k_{obs} plot showed saturation, K_d (dissociation constant) and k (first-order rate constant) were obtained (yielding the corresponding k^{app} values). See Supplementary Online Data for details of the kinetic studies.

Ferrocytochrome *c* and 1,4-dimethoxybenzene oxidation

Spectral changes during oxidation of ferrocytochrome *c* and 1,4-dimethoxybenzene were analysed with an Agilent 8453 diode-array spectrophotometer. Decay of ferrocytochrome *c* (15 μM), prepared as described previously [17], was followed-up at 550 nm in 20 mM sodium succinate (pH 4.0) containing 0.1 μM enzyme and 0.1 mM H_2O_2. 1,4-Benzoquinone formation from 1,4-dimethoxybenzene (0.2 mM) was followed-up at 245 nm in 20 mM sodium succinate (pH 3.5) containing the same amounts of enzyme and H_2O_2.

EPR measurements and simulations

H_2O_2 (10 equiv.) was added directly to EPR tubes containing 200 μM LiP in 20 mM sodium succinate (pH 4.5), 1 mM $CaCl_2$ and 0.1 M NaCl. The tubes were then immediately frozen in liquid N_2. CW-X-band (9.4 GHz) EPR measurements were carried out with a Bruker E500 Elexsys using the Bruker ER4122 SHQE cavity and an Oxford Helium continuous-flow cryostat (ESR900). Spin quantitation was performed by double integration of the experimental EPR radical signal compared with the resting-state iron signal. Magnetic properties were computed on the B3LYP/6-31G* geometry optimized structures at the B3LYP/TZVP level. The solvent effects were taken into account using the polarizable continuum model. DFT (density functional theory) calculations were carried out using Gaussian03 (http://www.lct.jussieu.fr/manuels/Gaussian03/home.htm). Magnetic parameters were computed for the radical species of the tyrosine–VA adducts estimated to be the most stable by quantum calculations (and for the VA cation radical). The calculated magnetic parameters were used to obtain EPR simulated spectra using EasySpin.

Computational methods: system setup, docking, MD, QM and QM/MM

System setup included processing of the *T. cervina* LiP co-ordinates (PDB code 3Q3U) with the preparation wizard available in Maestro. This and other cited programs are included in the Schrödinger suite (http://www.schrodinger.com/productsuite/1/). The side chain of Phe^{89}, invisible in the crystal structure, was added and, on the basis of their local environment, the protonation states of different residues were defined. Cavity exploration was performed with SiteMap, and VA docking was performed with Glide. MD calculations were performed with Desmond using an orthorhombic box, with a buffer solvent region of at least 10 Å (1 Å = 0.1 nm), and an ionic force of 0.15 M (53 Na^+ and 42 Cl^- ions). DFT QM optimizations were performed with Jaguar using different functionals and basis sets, and gas phase and solvation structures were obtained. Single point MP2 calculations were performed with Gaussian03 using the 6-31G** basis set. QM/MM

calculations were performed with QSite and all structures were optimized at the M06-2X/6-311G**/OPLS (optimized potential for liquid simulations) level. See Supplementary Online Data for details of the above computational studies.

Degradation of (simple and polymeric) lignin model compounds

A radiolabelled non-phenolic simple lignin model compound ([ring-^{14}C]4-ethoxy-3-methoxyphenylglycerol-β-guaiacyl ether) was treated with pristine LiP and VA-LiP in the presence of H_2O_2, and the resulting products were analysed by HPLC/liquid scintillation counting. A radiolabelled polymeric lignin model [^{14}C-labelled DHP (dehydrogenation polymer), 4.7 μg·ml^{-1}] [19] was treated with LiP (0.01 μM) under conditions described previously [20]. The experiments were performed at 25 °C, pH 4.5, with and without VA (10 mM) by adding H_2O_2 (7.5 and 0.3 mM in reactions with and without VA respectively) continuously over 24 h. Depolymerization was assessed by Sephadex LH-20 chromatography in N,N′-dimethylformamide/0.1 M LiCl and collected fractions were assayed for ^{14}C content by scintillation counting. See Supplementary Online Data for details.

RESULTS

LiP pre-treatment under different conditions

To establish the optimal conditions for *T. cervina* LiP activation, the enzyme was pre-incubated with different amounts of H_2O_2 in the presence/absence of VA and the relative activities (estimated from the maximum slope at 310 nm indicating veratraldehyde formation) and lag periods (defined as the time to the attainment of maximum slope) were compared. For the H_2O_2 and VA pre-treatment, the lag period decreased as the amount of H_2O_2 was increased, disappearing when 20 equiv. was added, whereas the activity changed little (Figure 1A). For the pre-treatment in the absence of VA, activity decreased as the H_2O_2 amount was increased (Figure 1B). In this case, the lag remained, and 10 equiv. H_2O_2 completely abolished VA oxidation.

To further investigate the effect of the H_2O_2 alone and H_2O_2 and VA treatments, two pre-treated LiPs were prepared: (i) VA-LiP obtained by pristine LiP pre-incubation with VA and 50 equiv. of H_2O_2 that oxidized VA without a lag; and (ii) H_2O_2-LiP obtained by pre-incubation with 20 equiv. of H_2O_2 alone that showed no activity towards VA. The Y181N variant was also pre-treated under the same conditions. After Superdex 75 chromatography, the final yields (for both native LiP and its Y181N variant) were ~70 % for VA-LiP and ~40 % for H_2O_2-LiP, relative to the initial amount of enzyme. Pre-treated LiPs showed identical electronic absorption spectra.

MS analyses of the pre-treated LiPs

MS was used to investigate the modifications in the protein moiety of the pre-treated LiPs. The *m/z* of VA-LiP estimated by MALDI–TOF-MS (Figure 2C) was 166 units higher than that of pristine LiP (Figure 2A), suggesting that one molecule of VA (molecular mass 168 Da) binds covalently. The *m/z* of H_2O_2-LiP (Figure 2B) was increased by 32 units, suggesting that two oxygen atoms were incorporated into the protein. By contrast, the *m/z* of pristine Y181N was unaffected by the pre-treatments, indicating that the above changes involve Tyr^{181}.

To investigate the self-catalytic modifications of *T. cervina* LiP in more detail, the different preparations were digested

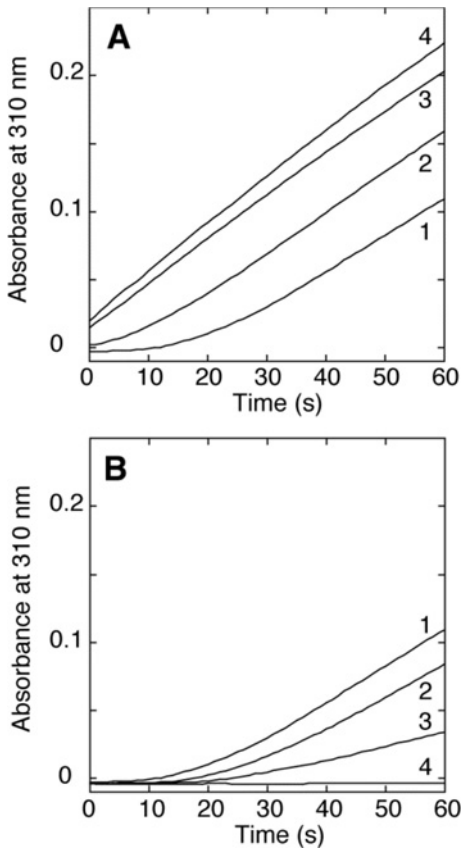

Figure 1 VA oxidation by *T. cervina* LiP pre-treated under different conditions

(**A**) Kinetic traces of VA oxidation to veratraldehyde (at 310 nm) by LiP pre-treated with 10 mM VA and 0 equiv. (line 1), 5 equiv. (line 2), 10 equiv. (line 3) and 20 equiv. (line 4) H_2O_2. (**B**) Kinetic traces of VA oxidation by LiP pre-treated with 0 equiv. H_2O_2 (line 1), 2 equiv. H_2O_2 (line 2), 5 equiv. H_2O_2 (line 3) and 10 equiv. H_2O_2 (line 4) in the absence of VA.

with Glu-C, and PMF and MS/MS sequencing analyses of the peptides obtained were performed by MALDI–TOF-MS. The PMF of pristine LiP shows several major ions consistent with the theoretical masses of the peptides expected, whose assignment was confirmed by MS/MS sequencing (as shown in Supplementary Figures S1 and S2 at http://www.biochemj.org/bj/452/bj4520575add.htm). The PMF profiles of H_2O_2-LiP and VA-LiP also contained the above ions except for that including Tyr^{181}. Instead of the *m/z* 1637.7 ion, the H_2O_2-LiP and VA-LiP PMF profiles showed new ions at *m/z* 1653.2 and 1803.7 with *m/z* increases of 16 and 166 units respectively.

Using the nLC-ESI-LTQ-Orbitrap Velos system (operating in CID mode), the Tyr^{181}-containing peptides from Glu-C digestion of pristine LiP (*m/z* 1637.7), LiP-H_2O_2 (*m/z* 1653.2) and VA-LiP (*m/z* 1803.7) were sequenced, yielding the sequence VVHLLASHSIAAQYE in pristine LiP, and the same sequence with modifications of Tyr^{181} in the two pre-treated LiPs. Owing to the nearly terminal position of Tyr^{181}, most of the $b+1$ ions were the same in the three samples, but the $y+1$ ions were different with constant *m/z* 16 and 166 increases in H_2O_2-LiP and VA-LiP respectively (as shown in Supplementary Figure S3 at http://www.biochemj.org/bj/452/bj4520575add.htm for VA-LiP compared with pristine LiP).

More precise information on the small $y+1$ ions from the above peptides containing the modified Tyr^{181} were obtained using the

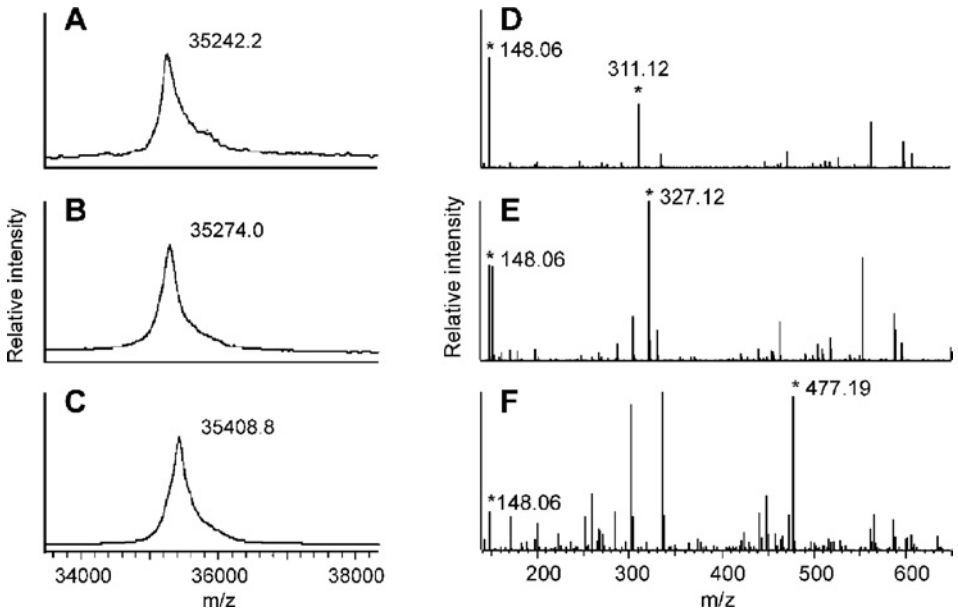

Figure 2 MS analyses of pristine LiP, H_2O_2-LiP and VA-LiP

Upper panels, pristine LiP; middle panels, H_2O_2-LiP; and lower panels, VA-LiP. (**A**–**C**) MALDI–TOF-MS of the whole protein; (**D**–**F**) nLC-MS/MS of the Tyr^{181}-containing peptide from Glu-C digestion. Pristine LiP (control) was pre-treated with 20 equiv. H_2O_2 in the absence of VA (H_2O_2-LiP) and in the presence of 10 mM VA (VA-LiP), and the three preparations were analysed. (**A**–**C**) Direct use of MALDI–TOF-MS showing *m/z* increases in H_2O_2-LiP (**B**) and VA-LiP (**C**) with respect to pristine LiP (**A**) (no *m/z* changes were observed in treated Y181N). (**D**–**F**) After Glu-C digestion, by MS using nLC-ESI-LTQ-Orbitrap Velos, where the peptides including Tyr^{181} in pristine LiP (triply charged at *m/z* 546.96), H_2O_2-LiP (triply charged at *m/z* 551.96) and VA-LiP (doubly charged at *m/z* 902.47) were fragmented (with the HCD) yielding singly charged ions at *m/z* 311.12 (dipeptide of Glu^{182} and unmodified Tyr^{181}) (**D**), *m/z* 327.12 (dipeptide of Glu^{182} and Tyr^{181} modified by H_2O_2) (**E**), and *m/z* 477.19 (dipeptide of Glu^{182} and Tyr^{181} modified by VA/H_2O_2) (**F**) respectively (the *m/z* 148.06 ion corresponding to Glu^{182} was also observed in the three cases).

MS/MS HCD mode of the nLC-ESI-LTQ-Orbitrap Velos system (Figures 2D–2F). By MS/MS fragmentation of the pristine-LiP peptide, singly charged ions at *m/z* 148.1 and 311.1 were detected (Figure 2D) corresponding to Glu^{182} and Tyr^{181}–Glu^{182} dipeptide respectively. MS/MS fragmentation of the corresponding H_2O_2-LiP peptide gave the same ion at *m/z* 148.1 and a second one at *m/z* 327.1 (Figure 2E) that corresponds to the dipeptide including modified Tyr^{181} together with Glu^{182}. Since the 179 *m/z* difference is 16 units higher than the mass of a tyrosine residue (163 Da in dehydrated form), the data confirm that one oxygen atom is introduced in Tyr^{181}. MS/MS fragmentation of the VA-LiP peptide gave singly charged ions at *m/z* 148.1 and 477.5 (Figure 2F). As in the case of H_2O_2-LiP, the former corresponds to the dipeptide including the modified Tyr^{181} together with Glu^{182} (and the latter to Glu^{182} alone). The 329.4 *m/z* difference, corresponding to the modified Tyr^{181}, is 166 units higher than the mass of a tyrosine residue, confirming that a VA molecule forms an adduct with Tyr^{181}.

Therefore it is possible to conclude that the two new peptides found after H_2O_2-LiP and VA-LiP digestions are derived from the Tyr^{181}-containing peptide detected after pristine LiP digestion, and that the *m/z* differences are due to Tyr^{181} modifications that incorporate: (i) one oxygen atom in H_2O_2-LiP to give a hydroxylated tyrosine residue (a second oxygen atom adds to an unidentified protein residue); and (ii) one VA molecule in VA-LiP to give a tyrosine–VA adduct.

Catalytic properties of the pre-treated LiPs

Steady-state kinetics of VA oxidation by VA-LiP yielded a k_{cat} of $17.1 \pm 0.8\ s^{-1}$, a K_m of 3.5 ± 0.4 mM and a catalytic efficiency (k_{cat}/K_m) of $4.8 \pm 0.1\ s^{-1} \cdot mM^{-1}$, whereas H_2O_2-LiP was unable to oxidize VA under steady-state conditions.

Additional information on the pre-treated LiPs was obtained using ferrocytochrome *c*, and 1,4-dimethoxybenzene. As shown in Figure 3(A), both H_2O_2-LiP and VA-LiP oxidize ferrocytochrome *c* to its ferric form. This indicates that both LiPs are able to form a catalytically active radical at the protein surface, since this large substrate cannot directly interact with the buried haem cofactor [21].

However, only VA-LiP could oxidize 1,4-dimethoxybenzene (Figure 3B). The negative result for H_2O_2-LiP indicates that activity towards this high-redox-potential substrate is lost after Tyr^{181} hydroxylation. The results of the present study agree with those obtained for VA, indicating that formation of the VA adduct is required for *T. cervina* LiP activity on high-redox-potential substrates.

Transient-state kinetics of the pre-treated LiPs

Transient-state kinetics for compound I formation by H_2O_2 and VA reduction of compounds I and II were investigated. The experiments, where a single turnover was investigated using the stopped-flow technique, enabled more precise comparison of VA-LiP and pristine LiP than the steady-state VA oxidation experiments, where multiple turnovers convert pristine LiP into VA-LiP in a few seconds.

Formation of compound I of both pristine and pre-treated LiPs exhibited a linear correlation between the k_{obs1} value and H_2O_2 concentration (Figure 4A). The very similar second-order rate constants (k_1^{app}) obtained (Table 1) indicate that the structural modifications caused by the pre-treatments do not affect the reaction mechanism with H_2O_2. However, large differences were observed for the VA reduction of compounds I and II.

When different VA concentrations were assayed, reduction of both compounds in pristine LiP showed a linear correlation

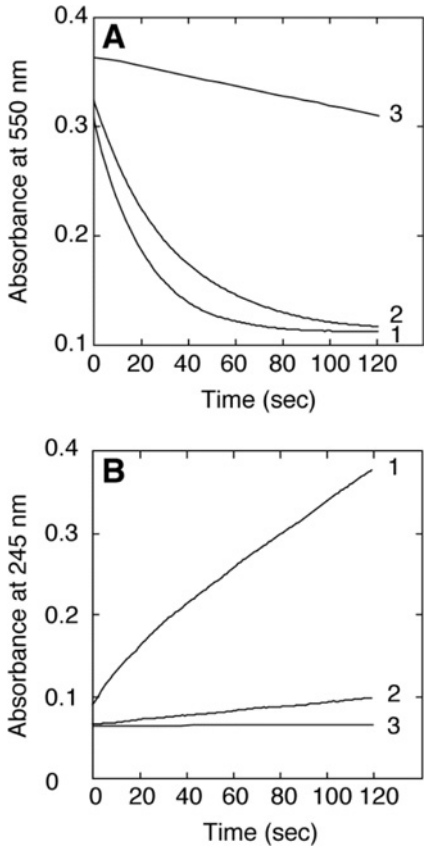

Figure 3 Oxidation of ferrocytochrome *c* and 1,4-dimethoxybenzene by the pre-treated LiPs

(**A**) Kinetic traces at 550 nm showing ferrocytochrome *c* decrease during its oxidation to ferricytochrome *c* by VA-LiP (line 1) and H_2O_2-LiP (line 2), compared with a control without enzyme (line 3). (**B**) Kinetic traces at 254 nm showing 1,4-benzoquinone formation during 1,4-dimethoxybenzene oxidation by VA-LiP (line 1) and H_2O_2-LiP (line 2), compared with a control without enzyme (line 3).

between k_{obs} and VA concentration, whereas in VA-LiP, saturating plots were observed (Figures 4B and 4C). This suggests that VA-LiP, when reacting with VA, forms a Michaelis–Menten ES (enzyme–substrate) complex. The apparent second-order rate constants for compounds I (k_2^{app}) and II (k_3^{app}) reduction by the three LiP preparations, together with the first-order rate (k_2) and dissociation (K_{D2}) constants for compound I reduction by VA-LiP (showing saturation kinetics) are provided in Table 2. The k_3^{app} values of pristine LiP and VA-LiP revealed that VA-LiP compound II has ~135-fold more activity when oxidizing VA than does pristine LiP (whereas k_2^{app} is much less affected, remaining on the same order as VA-LiP k_1^{app} and k_3^{app}). Compound II reduction is the rate-limiting step in pristine LiP catalysis, as shown by the low k_3^{app} value compared with the k_1^{app} and k_2^{app} values, and the improved compound II reactivity in VA-LiP explains the *T. cervina* LiP activation effect observed under steady-state conditions. The finding that the k_3^{app} for VA oxidation by VA-LiP is similar to the k_{cat}/K_m value obtained for pristine LiP under steady-state conditions also supports this idea.

Table 1 Transient-state kinetic constants (k_1^{app}) for compound I formation by H_2O_2

Means and 95 % confidence limits are shown.

Compound I formation	k_1^{app} ($\times 10^6$ $s^{-1} \cdot M^{-1}$)
Pristine LiP	3.3 ± 0.1
H_2O_2-LiP	2.5 ± 0.1
VA-LiP	2.4 ± 0.1

H_2O_2-LiP shows linear kinetics in compound I reduction by VA, as does pristine LiP (Figure 4B), but has a much lower (over 30-fold) k_{2app}. Moreover, H_2O_2-LiP compound II is not reduced by VA. This indicates that H_2O_2-LiP is unable to close its catalytic cycle using VA, which is consistent with its inability to oxidize VA (and 1,4-dimethoxybenzene) under steady-state conditions. The strongest effect of the two Tyr^{181} modifications was always found at the rate-limiting compound II reduction, resulting in strongly increased reactivity in the case of VA-LiP and complete lack of reactivity in H_2O_2-LiP.

VA docking and QM/MM calculations

Molecular docking and QM/MM calculations were performed to explore the existence of an encounter complex between VA and Tyr^{181}, and to study the oxidation at the encounter complex resulting in covalent binding.

SiteMap located a cavity directly on top of Tyr^{181}. The docking model from Glide XP (Figure 5A) shows VA between

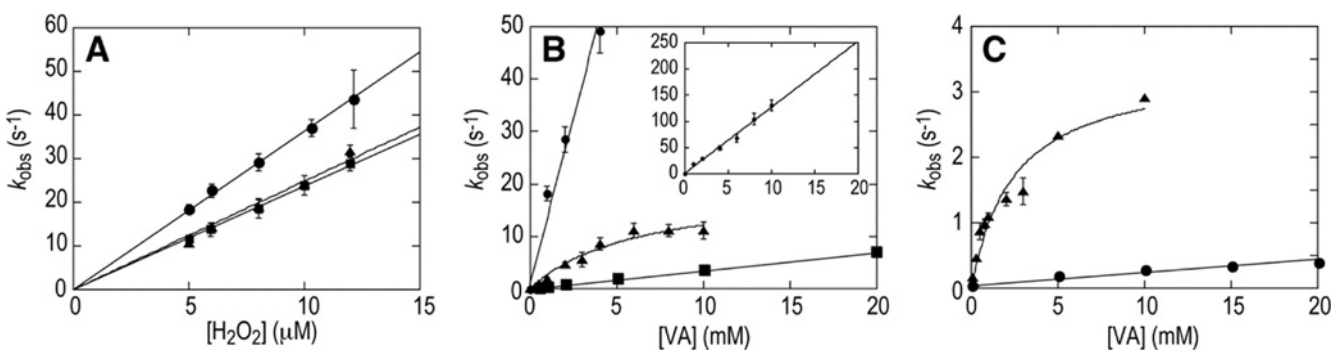

Figure 4 Transient-state kinetics for compound I formation and reduction of compounds I and II in pristine LiP, H_2O_2-LiP and VA-LiP

Plots of k_{obs} against substrate concentration show linear kinetics for compound I formation by H_2O_2 in the three enzyme preparations (**A**), pristine LiP and H_2O_2-LiP compound I reduction by VA (**B**), and pristine LiP compound II reduction by VA (**C**), whereas saturation kinetics are shown for the reduction of both VA-LiP compounds I and II by VA (**B** and **C** respectively). No plot for H_2O_2-LiP compound II reduction is shown in (**C**), since it cannot be reduced by VA. The inset shows the plot of pristine LiP compound I reduction at high VA concentrations. ●, LiP; ■, H_2O_2-LiP; ▲, VA-LiP. Error bars show means and 95 % confidence limits of replicate assays.

Table 2 Transient-state kinetic constants for compound II formation (k_2, K_{D2} and k_2^{app}) and reduction (k_3, K_{D3} and k_3^{app}) by VA

Means and 95 % confidence limits are shown. ND, not determined owing to linear correlations in [VA] compared with k_{obs}; nd, not determined owing to lack of activity.

Compound II formation	k_2 (s^{-1})	K_{D2} (mM)	k_2^{app} ($s^{-1} \cdot mM^{-1}$)	k_3 (s^{-1})	K_{D3} (mM)	k_3^{app} ($s^{-1} \cdot mM^{-1}$)
Pristine LiP	ND	ND	12.8 ± 0.1	ND	ND	0.02 ± 0.0
H_2O_2-LiP	ND	ND	0.35 ± 0.0	nd	nd	nd
VA-LiP	19.8 ± 2.5	6.3 ± 0.8	3.16 ± 0.4	1.9 ± 0.1	0.7 ± 0.1	2.7 ± 0.1

two aromatic residues, Tyr^{181} and Phe^{89}. Figure 5(A, inset) includes a DFT gas-phase model including Tyr^{181} and Phe^{89} side chains plus the VA ligand (optimized using the M06-2X functional) that clearly shows formation of a sandwich π stacking interaction, stabilizing the docked VA by means of dispersion forces. The geometry changes along the optimization mostly involve reorganization of the Phe^{89} side chain, which is not visible in the crystal structure. The interaction energies of the optimized structure at the DFT/M06-2X and the OPLS2005 force field theory levels are 14.3 and 9.8 kcal/mol respectively (quantum results corrected for basis set superimposition error). Thus, whereas the classical force field stabilizes the π complex, it considerably underestimates its strength. Figure 5(A, inset) also shows the spin density associated with the complex positive radical.

From the docking structure, we produced two 10 ns MD simulations where VA remained in the vicinity of Tyr^{181} for a significant fraction of the trajectory, 8 and 2 ns, before exiting into solution. The $Tyr^{181}(C_{\delta 2})$–$VA(C_\alpha)$ and $Phe^{89}(C_{\delta 1})$–$VA(C_\alpha)$ distances (Figure 5B, and Supplementary Movie S1 at http://www.biochemj.org/bj/452/bj4520575add.htm) show the formation of several stacking complexes along a trajectory segment.

For several MD snapshots describing stacking geometries, the compound I quartet and doublet spin states were modelled by QM/MM calculations (the QM region included the haem group, its axial ligands, VA, Tyr^{181} and Phe^{89}). All snapshots and spin states present two unpaired electrons in the iron-oxo moiety with an additional unpaired electron delocalized into the porphyrin ring, the VA ligand and Tyr^{181}. The spin density outside the haem group (Figure 5C), which agrees with the one obtained from the isolated stacked complex in its cation radical state (Figure 5A, inset), clearly involves the VA ligand and the side chain of Tyr^{181}. Thus we observe electron transfer from the Tyr^{181}–VA couple into the compound I porphyrin radical, giving compound II and a cation radical located in VA.

Quantum calculations were also performed to characterize the tyrosine–VA covalent binding. The optimized energy for several possible (C–C and ether) covalent adducts, modelling the tyrosine as the side-chain phenolic ring plus the C_β (as a methyl group), was computed. For all QM methods applied, compounds involving ring-to-ring covalent bonding are significantly more stable (for detailed results, see Supplementary Table S1 at http://www.biochemj.org/bj/452/bj4520575add.htm). In the gas phase, the tyrosine addition in the ortho-position with the phenolic OH was observed as the most stable structure, as expected from the tyrosine hydroxyl inductive effects. In continuum water, however, the inductive effects appear less important and both the ortho and meta substitutions are almost degenerate. In both cases (structures **C** and **F** in Supplementary Table S1), the VA C_6 is involved in the bond with the tyrosine molecule. Interestingly, in the QM-optimized structure after docking (Figure 5A, inset), the distance to form the above ortho addition (structure **F**), between tyrosine (C_3) and VA (C_6), is only 3.2 Å. Finally, QM calculations were performed to study spin distribution after one electron oxidation of the most probable tyrosine–VA adducts, structures **C** and **F** (Supplementary Table S1). The spin density is delocalized in both the tyrosine and VA moieties, with a higher concentration in VA.

EPR analysis of the pre-treated LiPs

The low temperature EPR spectra for the resting states of VA-LiP and H_2O_2-LiP are identical to that of pristine LiP (Figure 6A). This indicates that no significant modification occurs in the haem and its environment, which is consistent with the lack of significant changes in the absorption spectra and in the compound I formation rates.

However, after compound I formation with H_2O_2 significant differences were observed in the EPR spectra of the three LiP preparations. In all cases, peroxide activation results in disappearance of the strong iron(III) oxide signal dominating the EPR spectrum of the resting state, and the appearance of a new protein radical signal (Figure 6A). This protein radical signal in H_2O_2-LiP and VA-LiP shows different shape and intensity from that of pristine LiP, as shown in Figures 6(B) and 6(C) respectively (the radical yield under the experimental conditions used was estimated to be ~0.18 for pristine LiP, ~0.06 for H_2O_2-LiP and only ~0.008 spin/haem for VA-LiP).

The EPR spectrum of pristine LiP after peroxide activation is characterized by a typical tyrosyl radical signal, but that of H_2O_2-LiP shows a new radical signal that seems to consist of two different species (Figure 6B). One is assigned to a tyrosyl radical, whose presence is consistent with the existence of a certain percentage of unmodified Tyr^{181}, as found in the MS/MS analyses. The other, major species corresponds to a newly formed radical that could be assigned to a dopa radical. The detection of such a dopa radical agrees with the self-catalytic hydroxylation at Tyr^{181} shown by MS of the H_2O_2-LiP sample.

The EPR spectrum of peroxide-activated VA-LiP also shows the disappearance of the tyrosyl radical, and its substitution by a low intensity and poorly resolved new radical (Figure 6C). This confirms that Tyr^{181} is the site where VA reacts with the enzyme to form the tyrosine–VA adduct shown by MS of the VA-LiP sample. In agreement with the catalytic activation of VA-LiP described above, the new EPR signal in the peroxide-activated VA-LiP spectrum is consistent with a radical delocalized in the Tyr^{181} adduct including its VA moiety.

The experimental g_{iso} value (2.0036 ± 0.0002) agrees with the calculated g_{iso} values for the expected cationic structures (Supplementary Table S2 at http://www.biochemj.org/bj/452/bj4520575add.htm), showing that the tyrosine–VA adduct is in its cationic radical form. The calculated magnetic parameters show different coupling constants for the methylene hydrogens in VA when the addition to tyrosine is in the ortho- or meta-position in structures **F** and **C** as described above (Supplementary Table S1). The EPR simulation better fitting the signal observed in

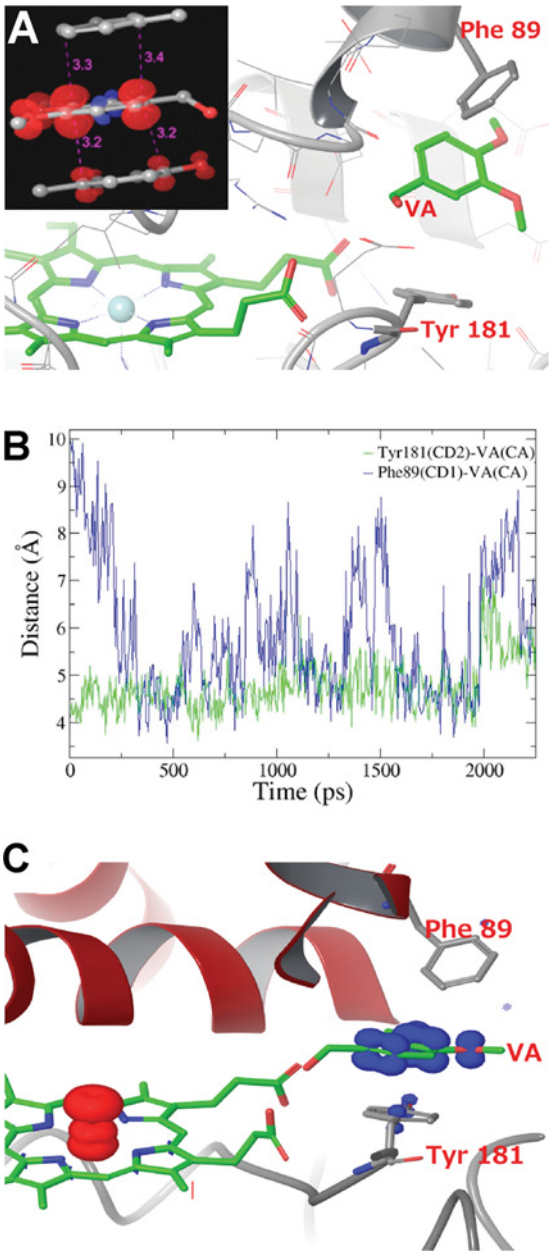

Figure 5 VA docking and sandwich π interaction, distances to Phe^{89} and Tyr^{181} during MD simulation, and porphyrin spin delocalization into Tyr^{181} and VA in one of the MD snapshots

(**A**) VA molecule docked on the *T. cervina* LiP crystal structure near Tyr^{181} and Phe^{89} using Glide XP (the inset shows a DFT gas-phase optimized structure revealing a sandwich π interaction of VA with the Phe^{89} and Tyr^{181} side chains, at 3.2–3.4 Å distances). (**B**) Tyr^{181}($C_{\delta 2}$)–VA(C_{α}) and Phe^{89}($C_{\delta 1}$)–VA(C_{α}) distances (green and blue lines respectively) during a 2.25 ns MD trajectory after VA docking, showing the high mobility of the Phe^{89} side chain and the formation of several stacking complexes with VA. (**C**) QM/MM calculations of spin densities for one snapshot from the above MD simulation showing partial spin delocalization giving rise to compound II and VA cation radical via Tyr^{181}.

peroxide-activated VA-LiP is consistent with structure **F** (Supplementary Table S2). For structure **C** the calculated coupling constants exceed the linewidth of the experimental spectrum. For the same reason, the EPR spectrum could not be assigned to the VA cation radical free in solution. Therefore structure- and EPR-based quantum calculations agree regarding the chemical

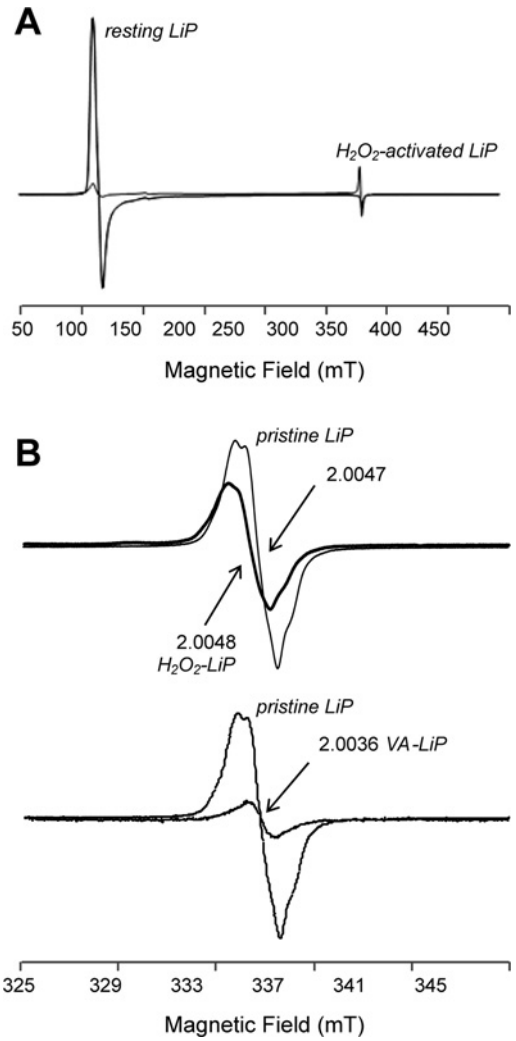

Figure 6 Low-temperature EPR spectra of resting state *T. cervina* LiP and protein radicals in peroxide-activated (compound I) pristine and pre-treated *T. cervina* LiPs

(**A**) Full-scan EPR spectrum of resting state and peroxide-activated H_2O_2-LiP [the resting state spectra of pristine LiP and VA-LiP were identical to that of H_2O_2-LiP (results not shown)]. (**B**) Close up of the radical signal in peroxide-activated H_2O_2-LiP compared with pristine LiP. (**C**) Close up of the radical signal in peroxide-activated VA-LiP compared with pristine LiP. The g_{iso} values of the three protein radicals are indicated. All the EPR spectra were recorded at T = 20K, under the following conditions: (i) pristine LiP, $\nu = 9.40$ GHz, 0.1 mT modulation amplitude and 0.2 mW microwave power; (ii) H_2O_2-LiP, $\nu = 9.40$ GHz, 0.2 mT modulation amplitude and 1 mW microwave power; and (iii) VA-LiP, $\nu = 9.40$ GHz, 0.4 mT modulation amplitude and 2 mW microwave power.

nature of the tyrosine–VA adduct formed during activation of the *T. cervina* LiP.

Oxidation of lignin model compound and polymeric lignin

To study the relevance of the activation mechanism in lignin degradation by *T. cervina* LiP, we first assessed the ability of pristine LiP and VA-LiP (H_2O_2-LiP was inactive on high-redox-potential compounds) to cleave a simple non-phenolic lignin model compound, 4-ethoxy-3-methoxy-phenylglycerol-β-guaiacyl ether, which includes the main (β-O-4) interunit linkage in lignin. The model compound was ^{14}C-labelled to facilitate detection and quantification of the oxidation/degradation products. VA-LiP oxidized the model compound

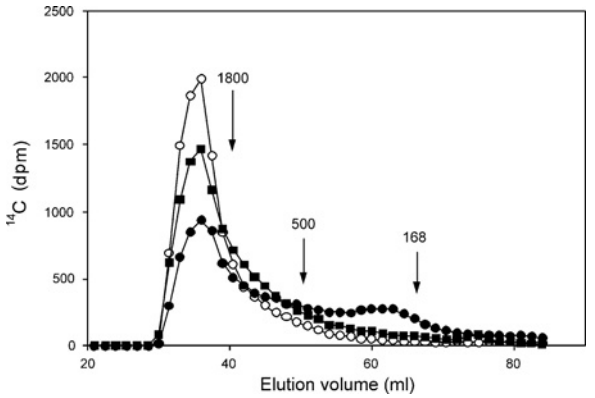

Figure 7 Gel permeation chromatograms of ^{14}C-labelled synthetic lignin (DHP) treated with VA-LiP in the presence (●) and absence (■) of VA

The result of a control reaction without enzyme (○) is also shown. Total recoveries of initially added ^{14}C were 78 % for DHP treated with VA-LiP both with and without VA. Recovery from the control without enzyme was somewhat higher as reported previously [20]. The arrows indicate elution volumes of two polystyrene molecular mass standards (1800 and 500 Da) and of VA (168 Da).

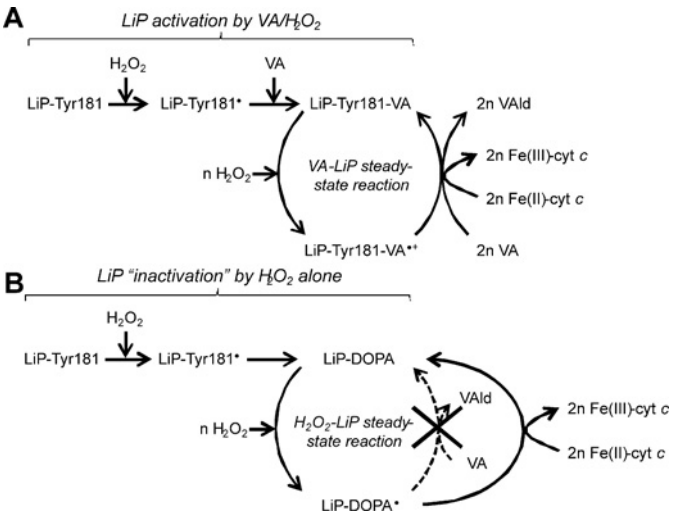

Figure 8 Schematic diagram of self-catalytic modifications (activation/inactivation) observed in *T. cervina* LiP

(**A**) LiP activation by VA and H_2O_2, during the first enzyme turnover, resulting in formation of a Tyr^{181}–VA adduct whose radical after peroxide activation (detected by EPR) would be responsible for the oxidation of the lignin model VA {and the low-redox-potential ferrocytochrome *c* [Fe(II)-cytc]} in subsequent turnovers (steady-state conditions). (**B**) LiP inactivation by H_2O_2 alone, during the first enzyme turnover, resulting in Tyr^{181} hydroxylation to a dopa residue whose semiquinone radical after peroxide activation (detected by EPR) was unable to oxidize VA (and lignin) in subsequent turnovers (steady-state conditions) although it is able to oxidize ferrocytochrome *c* owing to its low redox potential. VAld, veratryl aldehyde.

(Supplementary Figure S4, dashed line, at http://www.biochemj.org/bj/452/bj4520575add.htm) giving a 42 % yield of the cleavage product 4-ethoxy-3-methoxybenzaldehyde (Supplementary Figure S4, peak 2), and two minor additional cleavage products, 1-(4-ethoxy-3-methoxyphenyl)-2,3-dihydroxypropan-1-one (peak 4) and 1-(4-ethoxy-3- methoxyphenyl)glycerol (peak 5), together with 37 % of the C_α-oxidation ketone product (peak 3) (yields are relative to the limiting H_2O_2 concentration used). By contrast, very limited model compound breakdown (∼5 % aldehyde) was produced by pristine LiP (Supplementary Figure S4, dotted line) although oxidation of the model compound to the corresponding ketone (25 % yield) was observed. Those results show that the VA adduct provides a higher activity on lignin model compounds in *T. cervina* LiP, thus facilitating their C_α–C_β cleavage.

To obtain more direct evidence on the need for peroxidase activation in lignin degradation by *T. cervina* LiP, depolymerization of a ^{14}C-labelled synthetic lignin (DHP) by VA-LiP was investigated (Figure 7) by gel permeation chromatography after reactions in the presence (●) and absence (■) of VA, compared with a control reaction without enzyme (○) (the reactions were performed at pH 4.5 because LiPs are poorly stable during extended incubations at lower pH). VA-LiP released low-molecular-mass products from the DHP, as shown by the production of later-eluting products in the molecular mass distribution. The ability of VA-LiP to depolymerize the DHP in the absence of VA was detectable, but much lower. Finally, a slight extent of DHP depolymerization was observed using pristine LiP in the presence of VA (results not shown), perhaps because some of the enzyme was converted into VA-LiP during the reaction. The observations from the present study are consistent with the very low cleavage activity of pristine LiP towards the lignin model compound, as described above.

DISCUSSION

Ligninolytic organisms have developed a strategy for ligninolysis, a key step in terrestrial carbon recycling, on the basis of production of LiP and VP enzymes, whose common ancestral origin has been established recently [22]. This strategy implies the evolution in the above peroxidases of long-range electron transfer routes from protein radicals at the enzyme surface, which are able to abstract electrons from the bulky lignin polymer and transfer them on to the buried haem cofactor and ultimately to the oxidizing substrate (H_2O_2) [3]. In most of the above enzymes, an exposed tryptophan residue has a central role in the electron transfer pathways for lignin degradation. *T. cervina* LiP is thus far unique in containing a radical-forming exposed tyrosine (Tyr^{181}) in place of the conserved tryptophan [22]. The present study provides interesting and unexpected evidence on how the catalytic tyrosine works in *T. cervina* LiP, compared with the above-mentioned catalytic tryptophan residues. We have demonstrated that before being able to oxidize high-redox-potential substrates, including lignin, the enzyme must be activated by VA in the presence of H_2O_2. This activation causes a lag in the steady-state reactions, and a strong increase (over 100-fold) in the reactivity of LiP compound II with VA. Incidentally, we have also observed that H_2O_2-LiP results in enzyme inactivation by removing the above compound II reactivity.

Taking into consideration the catalytic properties of the above pre-treated LiPs (referred to as VA-LiP and H_2O_2-LiP in the present paper), together with the structural modifications observed and the results from computational simulations, the following activation/inactivation mechanisms are proposed for *T. cervina* LiP (Figure 8). The reaction with H_2O_2 alone causes hydroxylation of Tyr^{181} (to a dopa residue) that irreversibly abolishes the ability of the enzyme to oxidize high-redox-potential substrates (such as VA and 1,4-dimethoxybenzene), although the activity towards low-redox-potential large molecules (such as ferrocytochrome *c*) is unaffected. The same reaction, but in the presence of VA, yields a VA covalent adduct at Tyr^{181} that results in the functional activation of the enzyme. The computational simulations, optimized at the M06-2X/6-311G**/OPLS level that adequately describes π stacking interactions [23], reveal for the first time in a peroxidase that, a sandwich π stacking interaction between substrate (VA) and aromatic residues (LiP Tyr^{181} and Phe^{89}) plays a role in substrate binding and subsequent catalysis. QM/MM simulations,

an excellent tool to study the spin delocalization in peroxidase compound I [24], further reveal spin density at the VA–Tyr^{181} moiety. Thus one-electron oxidations are proposed to take place at the aromatic rings of VA and Tyr^{181}, causing deprotonation and ring–ring covalent bonding that yield the tyrosine–VA adduct, whose presence was unambiguously demonstrated by MS techniques. Direct oxidation of substrates in an environment, similar to the one discussed in the present study for VA, has been shown in ascorbate peroxidase [24].

The effects of the two LiP pre-treatments can be explained by considering the redox potential of the tyrosine modification products. We propose that the tyrosine–VA adduct (in VA-LiP) plays a role as a catalytic radical site that exhibits higher oxidation power than the intact Tyr^{181} radical, since VA possesses a higher redox potential (1.36 V) [12] than tyrosine (0.83 V at pH 7.0, and 1.15 V at pH 1.5) [25]. Conversely, hydroxylation of Tyr^{181} would decrease the oxidation power of the catalytic radical, since the dopa radical redox potential (0.56 V at pH 7.0, and 0.80 V at pH 1.5) [26] is lower than that of the tyrosine radical.

Those explanations are based not only on the computational simulation and on the structural and catalytic properties of the pristine and pre-treated LiPs, but also on their low-temperature EPR spectra. The latter directly demonstrated the presence of a tyrosine phenoxy radical in pristine LiP [17], and a dopa phenoxy radical in H_2O_2-LiP, which was assigned by comparison with the literature [27,28]. Moreover, the less resolved protein radical signal found in VA-LiP was compatible with a VA cation radical [11], shared with the tyrosine moiety of the Tyr^{181}–VA adduct. The above EPR spectra illustrate the differences between the *T. cervina* LiP mechanisms for electron abstraction from lignin compared with those found in other LiPs and VPs containing an exposed tryptophan residue, where a tryptophanyl radical is detected in the compound I spectrum [29,30]. The experimental EPR data, combined with magnetic parameter calculations on the possible structures predicted previously, also provide information on the chemical nature of the adduct formed between VA and *T. cervina* LiP Tyr^{181}.

To date, several autocatalytic modifications of peroxidases have been described, all of which are suggested to derive from protein radicals formed after enzyme reaction with H_2O_2. Among fungal peroxidases, *P. chrysosporium* LiP experiences β-hydroxylation of the catalytic Trp^{171} by reaction with H_2O_2 alone [31], although no significant effect of this self-modification on enzyme catalysis has been reported. In our previous study, it was shown by low-temperature EPR that *T. cervina* LiP produces the Tyr^{181} neutral radical after H_2O_2 activation [17], suggesting that the modifications observed in pre-treated LiPs would involve the Tyr^{181} radical. The novel and interesting aspect of the present study is that different structural modifications of *T. cervina* LiP result in the above-described opposite effects on LiP activity depending on the presence or absence of an aromatic substrate such as VA.

The irreversible removal of the activity towards high-redox-potential substrates caused by hydroxylation of Tyr^{181} (to a dopa residue) is a new H_2O_2-mediated inactivation mechanism different from the haem-bleaching inactivation described for other peroxidases [32]. On the other hand, the effect of VA on *T. cervina* LiP catalysis in preventing inactivation by H_2O_2, and providing a higher oxidation power to the enzyme, are reminiscent of the VA effects on *P. chrysosporium* LiP catalysis, where it acts as an enzyme protector against H_2O_2 inactivation by reverting compound III [13], and as a free cation radical mediator fixed at the Trp^{171} environment by electrostatic forces [12]. However, the VA structural and/or functional effects are different for both enzymes, and only *T. cervina* LiP requires formation of a Tyr^{181}–VA covalent adduct to be catalytically active on high-redox-potential substrates including lignin. In this context, it is important that our experiments with lignin models show that ligninolysis was catalysed only by activated LiP containing the VA adduct. That is to say, activation by VA is required for the ligninolytic activity of *T. cervina* LiP. Similar activation mechanisms could operate in other oxidoreductases that form tyrosine radicals involved in catalysis.

AUTHOR CONTRIBUTION

Yuta Miki performed most of the biochemical work. Rebecca Pogni, Maria Baratto, Adalgisa Sinicropi and Riccardo Basosi contributed to EPR experiments, simulations and interpretation of data. Sandra Acebes, Fátima Lucas and Victor Guallar contributed to molecular docking, QM/MM and other computational work. Elena Fernández-Fueyo and Kenneth Hammel performed lignin model degradation experiments. María Fernández and Vivian de los Ríos performed MS analyses, and Francisco Ruiz-Dueñas contributed to kinetic analyses. All authors participated in the interpretation and discussion of results. Victor Guallar and Angel Martínez contributed most of the data integration and writing, with assistance from Kenneth Hammel.

ACKNOWLEDGEMENTS

The authors thank Ignacio Casal [Proteomics and Genomics Facility at CIB (Centro de Investigaciones Biológicas)] and José C. del Río [IRNAS (Instituto de Recursos Naturales y Agrobiología de Sevilla), CSIC (Consejo Superior de Investigaciones Científicas)] for their help in the MS analyses, and Michael D. Mozuch for technical assistance with the DHP depolymerization reactions.

FUNDING

This work was supported by the Spanish projects BIO2008-01533 (to A.T.M.), CTQ2010-18123 (to V.G.) and BIO2011-26694 (to F.J.R.-D.) and the ProteoRed platform of the Spanish Institute of Health Carlos III (ISCIII); the Italian MIUR (PRIN 2009) project (to R.P. and R.B.); the European projects BIORENEW [grant number NMP2-CT-2006-026456 (to A.T.M.)], PELE [grant number ERC-2009-Adg 25027 (to V.G)] and PEROXICATS [grant number KBBE-2010-4-265397 (to A.T.M.)]; and the U.S. Department of Energy [grant number DE-AI02-07ER64480 (to K.E.H.). Y.M. and F.J.R.-D. thank the financial support of a European project contract, and a Ramón y Cajal contract of the Spanish Ministry of Economy and Competitiveness respectively.

REFERENCES

1 Ruiz-Dueñas, F. J. and Martínez, A. T. (2010) Structural and functional features of peroxidases with a potential as industrial biocatalysts. In Biocatalysts Based on Heme Peroxidases (Torres, E. and Ayala, M., eds), pp. 37–59, Springer-Verlag, Berlin

2 Martínez, A. T., Ruiz-Dueñas, F. J., Martínez, M. J., del Río, J. C. and Gutiérrez, A. (2009) Enzymatic delignification of plant cell wall: from nature to mill. Curr. Opin. Biotechnol. **20**, 348–357

3 Ruiz-Dueñas, F. J. and Martínez, A. T. (2009) Microbial degradation of lignin: how a bulky recalcitrant polymer is efficiently recycled in nature and how we can take advantage of this. Microb. Biotechnol. **2**, 164–177

4 de Jong, E., Field, J. A. and de Bont, J. A. M. (1994) Aryl alcohols in the physiology of ligninolytic fungi. FEMS Microbiol. Rev. **13**, 153–188

5 Shimada, M., Nakatsubo, F., Kirk, T. K. and Higuchi, T. (1981) Biosynthesis of the secondary metabolite veratryl alcohol in relation to lignin degradation by *Phanerochaete chrysosporium*. Arch. Microbiol. **129**, 321–324

6 Doyle, W. A., Blodig, W., Veitch, N. C., Piontek, K. and Smith, A. T. (1998) Two substrate interaction sites in lignin peroxidase revealed by site-directed mutagenesis. Biochemistry **37**, 15097–15105

7 Pérez-Boada, M., Ruiz-Dueñas, F. J., Pogni, R., Basosi, R., Choinowski, T., Martínez, M. J., Piontek, K. and Martínez, A. T. (2005) Versatile peroxidase oxidation of high redox potential aromatic compounds: site-directed mutagenesis, spectroscopic and crystallographic investigations of three long-range electron transfer pathways. J. Mol. Biol. **354**, 385–402

8 Ruiz-Dueñas, F. J., Pogni, R., Morales, M., Giansanti, S., Mate, M. J., Romero, A., Martínez, M. J., Basosi, R. and Martínez, A. T. (2009) Protein radicals in fungal versatile peroxidase: catalytic tryptophan radical in both compound I and compound II and studies on W164Y, W164H and W164S variants. J. Biol. Chem. **284**, 7986–7994

9 Bernini, C., Pogni, R., Basosi, R. and Sinicropi, A. (2012) The nature of tryptophan radicals involved in the long-range electron transfer of lignin peroxidase and lignin peroxidase-like systems: insights from quantum mechanical/molecular mechanics simulations. Proteins **80**, 1476–1483
10 Zapanta, L. S. and Tien, M. (1997) The roles of veratryl alcohol and oxalate in fungal lignin degradation. J. Biotechnol. **53**, 93–102
11 Khindaria, A., Nie, G. and Aust, S. D. (1997) Detection and characterization of the lignin peroxidase compound II–veratryl alcohol cation radical complex. Biochemistry **36**, 14181–14185
12 Khindaria, A., Yamazaki, I. and Aust, S. D. (1996) Stabilization of the veratryl alcohol cation radical by lignin peroxidase. Biochemistry **35**, 6418–6424
13 Wariishi, H. and Gold, M. H. (1990) Lignin peroxidase compound III: mechanism of formation and decomposition. J. Biol. Chem. **265**, 2070–2077
14 Miki, Y., Ichinose, H. and Wariishi, H. (2010) Molecular characterization of lignin peroxidase from the white-rot basidiomycete *Trametes cervina*: a novel fungal peroxidase. FEMS Microbiol. Lett. **304**, 39–46
15 Tomšovský, M. (2008) Molecular phylogeny and taxonomic position of *Trametes cervina* and description of a new genus *Trametopsis*. Ceska Mykol. **60**, 1–11
16 Miki, Y., Ichinose, H. and Wariishi, H. (2011) Determination of a catalytic tyrosine in *Trametes cervina* lignin peroxidase with chemical modification techniques. Biotechnol. Lett. **33**, 1423–1427
17 Miki, Y., Calviño, F. R., Pogni, R., Giansanti, S., Ruiz-Dueñas, F. J., Martínez, M. J., Basosi, R., Romero, A. and Martínez, A. T. (2011) Crystallographic, kinetic, and spectroscopic study of the first ligninolytic peroxidase presenting a catalytic tyrosine. J. Biol. Chem. **286**, 15525–15534
18 Miki, Y., Morales, M., Ruiz-Dueñas, F. J., Martínez, M. J., Wariishi, H. and Martínez, A. T. (2009) *Escherichia coli* expression and *in vitro* activation of a unique ligninolytic peroxidase that has a catalytic tyrosine residue. Protein Expression Purif. **68**, 208–214
19 Shary, S., Ralph, S. A. and Hammel, K. E. (2007) New insights into the ligninolytic capability of a wood decay ascomycete. Appl. Environ. Microbiol. **73**, 6691–6694
20 Hammel, K. E., Jensen, K. A., Mozuch, M. D., Landucci, L. L., Tien, M. and Pease, E. A. (1993) Ligninolysis by a purified lignin peroxidase. J. Biol. Chem. **268**, 12274–12281
21 Wariishi, H., Sheng, D. W. and Gold, M. H. (1994) Oxidation of ferrocytochrome *c* by lignin peroxidase. Biochemistry **33**, 5545–5552
22 Floudas, D., Binder, M., Riley, R., Barry, K., Blanchette, R. A., Henrissat, B., Martínez, A. T., Otillar, R., Spatafora, J. W., Yadav, J. S. et al. (2012) The Paleozoic origin of enzymatic lignin decomposition reconstructed from 31 fungal genomes. Science **336**, 1715–1719
23 Zhao, Y. and Truhlar, D. G. (2008) The M06 suite of density functionals for main group thermochemistry, thermochemical kinetics, noncovalent interactions, excited states, and transition elements: two new functionals and systematic testing of four M06-class functionals and 12 other functionals. Theor. Chem. Acc. **120**, 215–241
24 Guallar, V. (2008) Heme electron transfer in peroxidases: the propionate e-pathway. J. Phys. Chem. B **112**, 13460–13464
25 Tommos, C., Skalicky, J. J., Pilloud, D. L., Wand, A. J. and Dutton, P. L. (1999) *De novo* proteins as models of radical enzymes. Biochemistry **38**, 9495–9507
26 Chen, S.-M. and Peng, K.-T. (2012) The electrochemical properties of dopamine, epinephrine, norepinephrine, and their electrocatalytic reactions on cobalt(II) hexacyanoferrate films. J. Electroanal. Chem. **547**, 179–189
27 Seyedsayamdost, M. R. and Stubbe, J. (2006) Site-specific replacement of Y356 with 3,4-dihydroxyphenylalanine in the β2 subunit of *E. coli* ribonucleotide reductase. J. Am. Chem. Soc. **128**, 2522–2523
28 Chen, Y., Chen, C., Chen, W., Zweier, J. L., Augusto, O., Radi, R. and Mason, R. P. (2004) Formation of protein tyrosine ortho-semiquinone radical and nitrotyrosine from cytochrome *c*-derived tyrosyl radical. J. Biol. Chem. **279**, 18054–18062
29 Pogni, R., Baratto, M. C., Giansanti, S., Teutloff, C., Verdín, J., Valderrama, B., Lendzian, F., Lubitz, W., Vázquez-Duhalt, R. and Basosi, R. (2005) Tryptophan-based radical in the catalytic mechanism of versatile peroxidase from *Bjerkandera adusta*. Biochemistry **44**, 4267–4274
30 Pogni, R., Baratto, M. C., Teutloff, C., Giansanti, S., Ruiz-Dueñas, F. J., Choinowski, T., Piontek, K., Martínez, A. T., Lendzian, F. and Basosi, R. (2006) A tryptophan neutral radical in the oxidized state of versatile peroxidase from *Pleurotus eryngii*: a combined multi-frequency EPR and DFT study. J. Biol. Chem. **281**, 9517–9526
31 Blodig, W., Doyle, W. A., Smith, A. T., Winterhalter, K., Choinowski, T. H. and Piontek, K. (1998) Autocatalytic formation of hydroxy group at Cβ of Trp^{171} in lignin peroxidase. Biochemistry **37**, 8832–8838
32 Valderrama, B., Ayala, M. and Vázquez-Duhalt, R. (2002) Suicide inactivation of peroxidases and the challenge of engineering more robust enzymes. Chem. Biol. **9**, 555–565

Received 18 February 2013/28 March 2013; accepted 3 April 2013
Published as BJ Immediate Publication 3 April 2013, doi:10.1042/BJ20130251

Biochem. J. (2013) **452**, 575–584 (Printed in Great Britain) doi:10.1042/BJ20130251

online data multimedia

SUPPLEMENTARY ONLINE DATA

Formation of a tyrosine adduct involved in lignin degradation by *Trametopsis cervina* lignin peroxidase: a novel peroxidase activation mechanism

Yuta MIKI*[1], Rebecca POGNI†, Sandra ACEBES‡, Fátima LUCAS‡, Elena FERNÁNDEZ-FUEYO*, Maria Camilla BARATTO†, María I. FERNÁNDEZ*, Vivian DE LOS RÍOS*, Francisco J. RUIZ-DUEÑAS*, Adalgisa SINICROPI†, Riccardo BASOSI†, Kenneth E. HAMMEL§, Victor GUALLAR‡‖ and Angel T. MARTÍNEZ*[2]

*Centro de Investigaciones Biológicas, CSIC, Ramiro de Maeztu 9, E-28040 Madrid, Spain, †Department of Biotechnologies, Chemistry and Pharmacy, University of Siena, I-53100 Siena, Italy, ‡Joint BSC-IRB Research Program in Computational Biology, Barcelona Supercomputing Center, Jordi Girona 29, E-08034 Barcelona, Spain, §USDA Forest Service, Forest Products Laboratory, One Gifford Pinchot Drive, Madison, WI 53726, U.S.A., and ‖Institució Catalana de Recerca i Estudis Avançats (ICREA), Passeig Lluís Companys 23, E-08010 Barcelona, Spain

MATERIALS AND METHODS

MS analyses

Molecular masses of pristine and pre-treated LiP proteins were analysed by MALDI–TOF-MS using an Autoflex III MALDI–TOF/TOF instrument (Bruker Daltonics). The same volumes of protein solution, 2 % TFA (trifluoroacetic acid) and 2 % 2,5-dihydroxyacetophenone matrix were mixed, and 1 μl was spotted on to an 800 μm AnchorChip MALDI probe. Spectra were acquired using a laser power just above the ionization threshold, and were analysed in the positive ion detection and delayed extraction linear mode (1000 laser shots were typically summed). External calibration was performed covering the range 15 000–70 000 Da.

For peptide analysis, LiP samples (200 ng $\cdot$ μl^{-1}) were digested with Glu-C endoprotease (10 ng $\cdot$ μl^{-1}) in 100 μl of 0.5× Glu-C reaction buffer (New England Biolab) at 25 °C for 16 h. The reaction mixtures were dried and dissolved in 0.1 % TFA, followed by ZipTip (Millipore) purification. The peptides were yielded in 10 μl of 70 % acetonitrile containing 0.1 % TFA. A sample of 1 μl was deposited on to the 800 μm AnchorChip and, when dried, 1 μl of saturated α-cyano-4-hydroxycinnamic acid matrix was added. Samples were analysed with the Autoflex III TOF/TOF mass spectrometer. Typically, 1000 scans for PMF and 2000 scans for tandem MS were collected. External calibration was performed (800–3200 Da) and analysis of data was carried out using the FlexAnalysis software.

Additionally, the peptide mixtures were analysed by online nLC-MS/MS on an EASY-nLC™ system connected to the LTQ Orbitrap Velos instrument (Thermo Fisher Scientific) through a Proxeon nanoelectrospray ion source. The peptides were dissolved in 5 μl of 2 % acetonitrile in 0.1 % formic acid, loaded on to a 2-cm C18-A1 precolumn and eluted on to a Biosphere C18 column (75 μm × 15 cm, 3 μm particle size) using a 45 min gradient of 2–95 % acetonitrile in 0.1 % formic acid at a flow rate of 250 nl $\cdot$ min^{-1}. The effluent was directly electrosprayed into the mass spectrometer. The LTQ instrument was operated in data-dependent mode to automatically switch between full scan MS and tandem MS acquisition. Instrument control was through Tune 2.6.0 and Xcalibur 2.1. Full-scan spectra were acquired with a target value of one million at a resolution of 60 000 at *m*/*z* 400 and the 15 most intense ions were selected for subsequent fragmentation. The normalized collision energy was set to 35 % for both CID and HCD. Precursor ion charge state screening and monoisotopic precursor selection were enabled and singly charged ions and unassigned charge states were rejected. Dynamic exclusion was enabled with a repeat count of 1 and an exclusion duration of 30 s. Raw files were searched against an in-house database using the SEQUEST search engine through Proteome Discoverer. Precursor and fragment mass tolerance were set to 10 p.p.m. and 0.8 Da respectively. Identified peptides were filtered by a false discovery rate of 0.01 using Percolator. After fragments of the peptide were elucidated, the identification of modification sites was confirmed through manual inspection of fragmentation spectra of modified peptides.

Kinetic studies

Steady-state kinetic constants for VA oxidation were estimated from veratraldehyde (ε_{310} = 9.3 mM^{-1} $\cdot$ cm^{-1}) formation in 20 mM sodium succinate containing 50 nM enzyme, and 0.1 mM H_2O_2. The reaction was performed at optimal pH 3.5. The K_m and k_{cat} values were obtained by non-linear least-squares fitting of the experimental values {reaction rates v and [S] (substrate concentrations)} to the Michaelis–Menten equation, $v = (k_{cat}/K_m)[S]/(1 + [S]/K_m)$. All the above reactions were carried out at 25 °C, and initiated by the addition of H_2O_2.

Transient-state kinetics was studied using a stopped-flow device equipped with a SFM 300 three-syringe module (Bio-Logic) and a MOS-DA diode-array detector (J&M Analytik). Compound I formation (confirmed using the diode-array detector) was studied by mixing the resting enzyme with different H_2O_2 concentrations under pseudo-first-order conditions. Kinetic constants were estimated from absorbance at 399 nm (compounds I and II isosbestic point).

To study compound II formation during VA oxidation, compound I was first formed by mixing resting enzyme and 1 equiv. H_2O_2. After full compound I formation (typically 40 ms for pristine LiP and 1.5 s for VA-LiP and H_2O_2-LiP), an excess of VA (more than 125 equiv.) was added, and compound II formation was confirmed using the diode-array detector. Kinetic constants were estimated from absorbance at 416 nm (isosbestic point of compound II and resting state).

For compound II reduction study, compound II was first formed by mixing resting enzyme with a solution containing 1 equiv. H_2O_2 and 1 equiv. sodium ferrocyanide. After full compound II

[1] Present address: Toyama Prefectural University, 5180 Kurokawa, Imizu, Toyama 939–0398, Japan.
[2] To whom correspondence should be addressed (email ATMartinez@cib.csic.es).

formation (1 s for pristine LiP and 5 s for VA-LiP and H_2O_2-LiP), an excess of VA (more than 125 equiv.) was added, and compound II reduction was confirmed using the diode-array detector. Kinetic constants were estimated from absorbance at 407 nm (Soret maximum of resting state).

All the above reactions were performed at 25 °C in 20 mM sodium succinate [pH 3.5 (the optimal for VA oxidation)], containing 1 μM enzyme, and exhibited single exponential kinetic traces giving k_{obs} values. When the plot of [S] against k_{obs} showed linear dependence, a k_{app} value with its S.E.M. were obtained from the linear fit using the equation $k_{obs} = k_{app} \times [S]$. When the plot of [S] against k_{obs} showed saturation, K_D and k values with their S.E.M. values were determined from non-linear fit using the Michaelis–Menten equation $k_{obs} = k/(1 + K_D/[S])$. Fitting of these constants to the normalized equation $v = (k/K_D)[S]/(1 + [S]/K_D)$ yielded the k_{app} values, with their corresponding S.E.M.

Computational methods: system setup, docking, MD, QM and QM/MM

The initial co-ordinates of the *T. cervina* LiP (PDB code 3Q3U) [1] were processed with the preparation wizard available in Maestro (http://www.schrodinger.com/productpage/14/12/). First, the side chain of Phe[89], non-visible in the crystal structure, was added. Then, on the basis of their local environment in the crystal structure, the protonation states of different residues were defined. In particular, Glu[40] and Glu[230] were neutralized (all other glutamic, aspartic, lysine and arginine residues kept their charged states), His[47] and His[175] were N_δ protonated, His[101], His[170] and His[210] were N_ε protonated, and His[39] was protonated in both nitrogen atoms. Previous to the cavity search for VA docking, a quick minimization using the OPLS2005 force field, a SGB (surface generalized born) solvent model, and a 0.1 root mean square gradient, were performed with Prime to eliminate any possible steric clash. Along with minimization, the iron centre and its co-ordinated atoms were kept frozen.

Cavity exploration was performed with SiteMap (http://www.schrodinger.com/productpage/14/20/), and VA docking was performed with Glide using the extra precision settings [2]. MD calculations were performed with Desmond [3]. The structures were solvated in an orthorhombic box, with a buffer solvent region of at least 10 Å. The system was then neutralized, and an ionic force of 0.15 M was set by adding 53 Na^+ and 42 Cl^- ions. The default relaxation protocol in Desmond was used followed by production runs using the NPT (moles, pressure and temperature) ensemble with a Nosé-Hoover thermostat and a Martyna–Tobias–Klein barostat. The temperature was set to 26.9 °C with a 2 fs time-step, shake on hydrogen atoms and long-range Ewald summation. The charges for the haem group and the VA ligand were obtained from the QM/MM electrostatic potential fitting for the docked structure.

DFT QM optimizations were performed with Jaguar (http://www.schrodinger.com/productpage/14/7/) using different functionals (M06, B3LYP and MPW1K) and basis sets (6-31G** and 6-311G**+). Gas-phase and solvation structures, using Jaguar's Poisson–Boltzmann solver, were obtained. Single-point MP2 calculations were performed with Gaussian03 using the 6-31G** basis set. The QM/MM calculations were performed with QSite (http://www.schrodinger.com/productpage/14/19/) and all structures were optimized at the M06-2X/6-311G**/OPLS level. The QM/MM systems were built from the fully solvated protein after removing all water molecules beyond 10 Å from any protein atom. Furthermore, all atoms beyond 20 Å from the haem CHA atom were constrained along the geometry optimizations.

Degradation of (simple and polymeric) lignin model compounds

Ring-^{14}C-labelled (1.0 mCi · mmol^{-1}) 4-ethoxy-3-methoxyphenylglycerol-β-guaiacyl ether was prepared as described previously [4]. The radiolabelled model compound (1 mM) was treated with pristine LiP and VA-LiP (H_2O_2-LiP has no activity) in 10 mM sodium acetate (pH 3.5) containing 0.25 mM H_2O_2 at 25 °C for 1 h. The products formed were analysed by reversed phase HPLC using a Gilson system equipped with a C18 column [Phenomenex Luna C18(2); 150 × 4.6 mm, 5 μm particle size] and methanol/water as mobile phase (35:65 for 15 min, followed by 50:50) at a flow rate of 1 ml · min^{-1}. Elution was monitored at 255 nm, and the ^{14}C content in collected fractions (0.5 ml) was measured in a liquid scintillation counter. HPLC in conjunction with GLC/MS was used in parallel analyses with unlabelled model compounds to confirm the identity of the products obtained.

Radiolabelled DHP with a syringyl/guaiacyl ratio of approximately 4:1 was prepared by enzymatic co-polymerization of β-[^{14}C]sinapyl alcohol (0.01 mCi · mmol^{-1}) and unlabelled coniferyl alcohol using horseradish peroxidase, and a high-molecular-mass fraction ($\geqslant$2 kDa) was obtained by Sephadex LH-20 chromatography [5]. Enzymatic depolymerization of the DHP by pristine LiP and VA-LiP (H_2O_2-LiP has no activity) was analysed as described previously [6]. The experiments were performed in 10 mM sodium acetate (pH 4.5) containing 0.25 % Tween 20, 1.5×10^4 d.p.m. (188 μg) DHP and 0.01 μM enzyme in a volume of 40 ml, in the presence or absence of 10 mM VA. Reactions were conducted at 25 °C by adding H_2O_2 continuously over 24 h (7.5 and 0.3 mM concentration in experiments with and without VA respectively). Control reactions without enzyme were performed. The reaction mixtures were concentrated by rotary vacuum evaporation, redissolved in N,N'-dimethylformamide containing 0.1 M LiCl and then centrifuged. Molecular mass distributions of the supernatant fractions were assessed on a 1.8 × 30-cm column of Sephadex LH-20, using N,N'-dimethylformamide containing 0.1 M LiCl as the mobile phase. Fractions (2 ml) were collected and assayed for ^{14}C in a liquid scintillation counter.

RESULTS

Four Supplementary Figures show MALDI–TOF PMF of the three LiP preparations digested with Glu-C (Figure S1), subsequent MALDI–TOF tandem MS sequencing of peptides from pristine LiP (Figure S2), high-resolution nLC-MS/MS sequencing of the Tyr[181]-containing peptide in pristine LiP and VA-LiP (Figure S3) and degradation of non-phenolic lignin model compound (Figure S4); and two Supplementary Tables present the energy differences for ten possible Tyr[181]–VA covalent adducts (Table S1), and the isotropic g values and coupling constants for the most probable Tyr[181]–VA adducts together with the EPR simulation for one of them (Table S2). Movie S1 shows an MD trajectory of VA establishing several stacking interactions with the side chains of Tyr[181] and Phe[89].

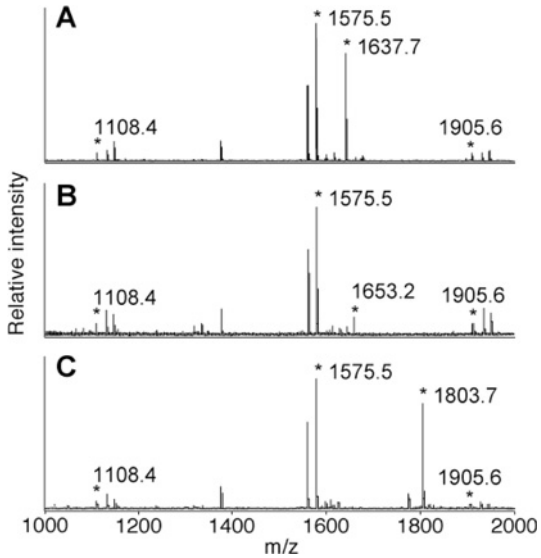

Figure S1 MALDI–TOF PMF (*m/z* 1000–2000) of Glu-C-digested pristine LiP, H_2O_2-LiP and VA-LiP

The peptides obtained by Glu-C digestion of the three LiP preparations were analysed by MALDI–TOF-MS using α-cyano-4-hydroxycinnamic acid matrix (asterisks indicate the ions of which the MS/MS sequencing is shown in Figure S2). The peptide including Tyr^{181} shows *m/z* 1637.7 in the pristine LiP (**A**), *m/z* 1653.2 (+ 16 with respect to pristine LiP) in the H_2O_2-LiP (**B**) sample, and *m/z* 1803.7 (+ 166 with respect to pristine LiP) in the VA-LiP (**C**) sample.

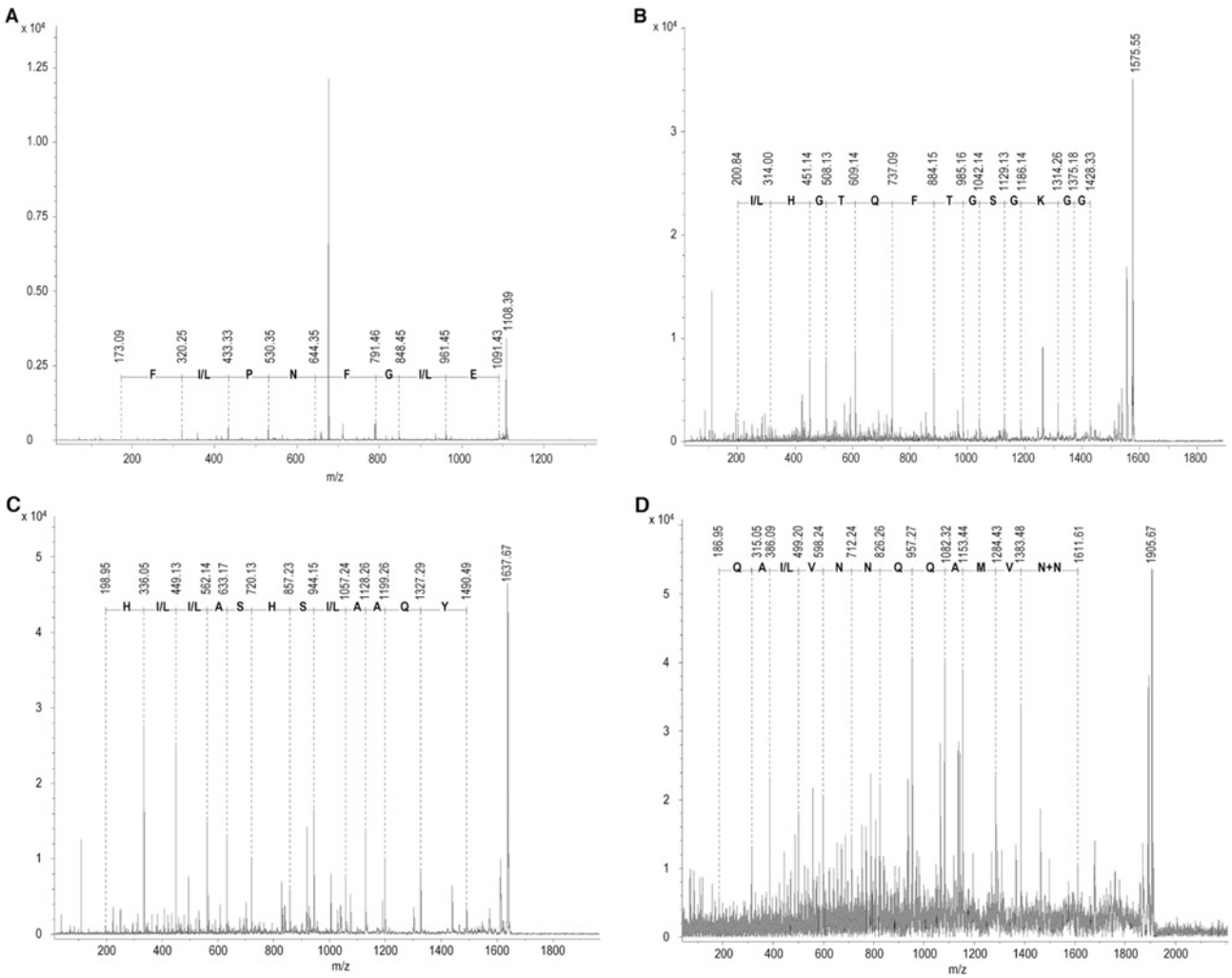

Figure S2 MALDI–TOF-tandem MS sequencing of the main peptides with *m/z* 1108.4, 1575.5, 1637.7 and 1905.6 from PMF of pristine LiP digested with Glu-C endoprotease (Figure S1A)

MALDI–TOF-MS/MS partially confirmed the amino acid sequences of the main peptides from PMF of pristine LiP with *m/z* 1108.4 (Thr^{79} to Glu^{88}) (**A**), 1575.5 (Ser^{207} to Glu^{222}) (**B**), 1637.7 (Val^{168} to Glu^{182}) (**C**) and 1905.6 (Trp^{249} to Glu^{264}) (**D**).

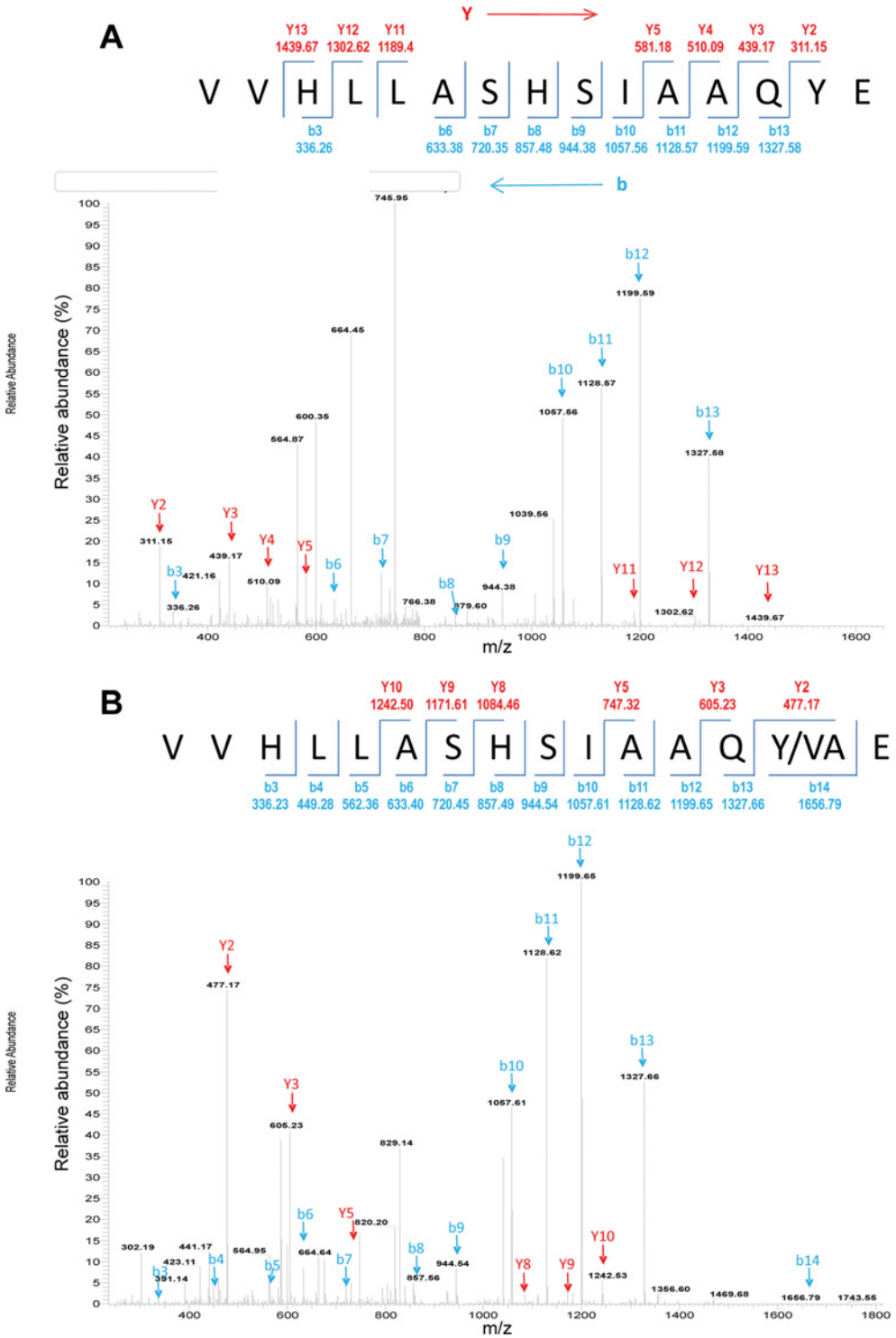

Figure S3 High-resolution nLC-MS/MS sequencing of the Tyr^{181}-containing LiP peptide showing tyrosine modification by VA/H_2O_2

(**A**) Sequencing of the Tyr^{181} peptide from pristine LiP (VVHLLASHSIAAQYE). (**B**) Sequencing of the VA-LiP peptide [VVHLLASHSIAAQ(Y/VA)E] with Tyr^{181}–VA adduct. Owing to the nearly terminal position of Tyr^{181}, most of the $b+1$ ions were the same in both samples (as well as in H_2O_2-LiP) including b_3, m/z 336; b_4, m/z 449; b_5, m/z 562; b_6, m/z 633; b_7, m/z 720; b_8, m/z 857; b_9, m/z 944; b_{10}, m/z 1058; b_{11}, m/z 1129; b_{12}, m/z 1200; and b_{13}, m/z 1328. However, the $y+1$ ions in the pristine LiP (y_2, m/z 311; y_3, m/z 439; y_4, m/z 510; y_5, m/z 581; y_6, m/z 694; etc.) and VA-LiP peptides (y_2, m/z 477; y_3, m/z 605; y_4, m/z 676; y_5, m/z 747; y_6, m/z 860; etc.) were different with constant m/z 166 increases (the $y+1$ ions were also different in H_2O_2-LiP, but with m/z 16 increases).

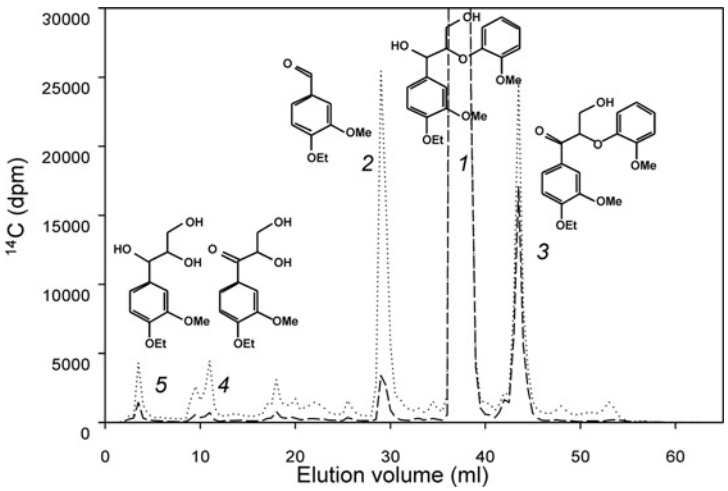

Figure S4 Degradation of non-phenolic lignin model compound

HPLC analysis of ^{14}C-labelled 4-ethoxy-3-methoxyphenylglycerol-β-guaiacyl ether (peak 1) degradation by pristine LiP (dashed line) and VA-LiP (dotted line) showing 4-ethoxy-3-methoxybenzaldehyde (peak 2), 1-(4-ethoxy-3-methoxyphenyl)-3-hydroxy-2-(2-methoxyphenoxy)-propan-1-one (peak 3), 1-(4-ethoxy-3-methoxyphenyl)-2,3-dihydroxypropan-1-one (peak 4) and 1-(4-ethoxy-3-methoxyphenyl)glycerol (peak 5) as the main products. Total recoveries of initially added ^{14}C from complete reactions were 88 and 94 % for model compound treated with pristine LiP and VA-LiP respectively.

Table S1 Quantum calculation of energy differences (kcal · mol^{-1}) for ten Tyr^{181}–VA adducts estimated in gas phase (MO6 or MP2 functionals) and solution (MO6)

The bond nomenclature in parentheses indicates the tyrosine side chain (modelled as a p-methylphenol molecule) and VA aromatic carbons respectively, forming the different C–C and ether bonds.

Structures (Tyr to VA bond)	Gas phase (MO6/6-31G**)	Gas phase (MP2/6-31G**)	Solution (MO6/6-31G**)
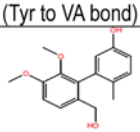 **A** (2-2')	5.2	1.8	2.8
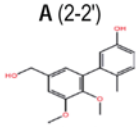 **B** (2-5')	5.2	2.3	2.4
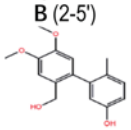 **C** (2-6')	2.8	2.9	0.0
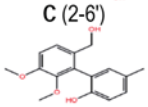 **D** (3-2')	1.3	0.6	2.9
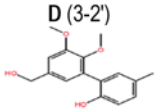 **E** (3-5')	3.0	3.2	2.9
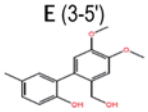 **F** (3-6')	0.0	0.0	0.1
 **G** (4-O-2' ether)	12.0	10.3	17.8
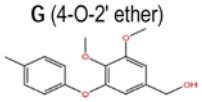 **H** (4-O-5' ether)	14.2	12.5	17.6
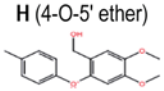 **I** (4-O-6' ether)	10.3	11.1	14.5
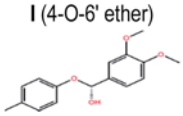 **J** (4-O-α' ether)	5.0	3.04	10.6

Table S2 B3LYP/TZVP isotropic *g* values and principal isotropic hyperfine coupling constants for C•+ (2–6′), F•+ (3–6′), F• (3-6′) and VA•+ species (see Supplementary Table S1), and EPR spectrum simulation for species F•+ (3–6′)

Coupling constants are given in mT and the average value for methyl protons are reported. Bulk solvent effects have been taken into account by using PCM. Experimental EPR spectrum of VA-LiP radical species (black) paired with the simulation (red) obtained with the calculated magnetic parameters reported for species F•+ (3–6′). The simulation has been performed with the Easyspin software package [7] using the 'pepper' function.

Structures			g_{iso}	A $H_{1'\text{-}CH2}$	A $H'_{1'\text{-}CH2}$	A $H_{3'\text{-}CH3}$	A $H_{4'\text{-}CH3}$
C•+ (2-6')	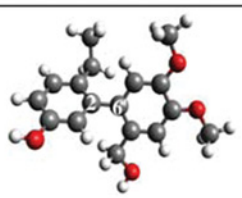		2.0037	1.55	1.15	0.31	0.28
F•+ (3-6')	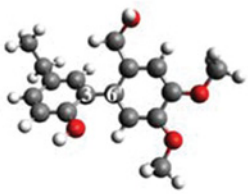	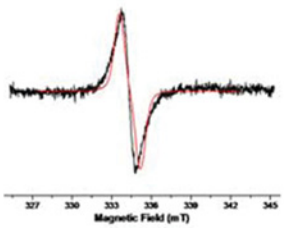	2.0036	1.04	0.38	0.27	0.20
			g_{iso}	A $H_{1'\text{-}CH}$	A $H_{2'}$	A $H_{5'}$	
F• (3-6')	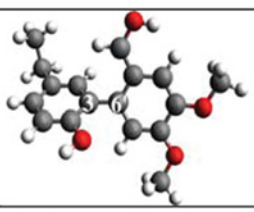		2.0032	1.54	0.42	0.21	
			g_{iso}	A $H_{1\text{-}CH2}$	A $H'_{1\text{-}CH2}$	A $H_{3'\text{-}CH3}$	A $H_{4'\text{-}CH3}$
VA•+	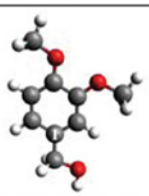		2.0038	1.68	1.68	0.31	0.34

REFERENCES

1 Miki, Y., Calviño, F. R., Pogni, R., Giansanti, S., Ruiz-Dueñas, F. J., Martínez, M. J., Basosi, R., Romero, A. and Martínez, A. T. (2011) Crystallographic, kinetic, and spectroscopic study of the first ligninolytic peroxidase presenting a catalytic tyrosine. J. Biol. Chem. **286**, 15525–15534

2 Friesner, R. A., Murphy, R. B., Repasky, M. P., Frye, L. L., Greenwood, J. R., Halgren, T. A., Sanschagrin, P. C. and Mainz, D. T. (2006) Extra precision glide: docking and scoring incorporating a model of hydrophobic enclosure for protein-ligand complexes. J. Med. Chem. **49**, 6177–6196

3 Bowers, K. J., Chow, E., Xu, H., Dror, R. O., Eastwood, M. P., Gregersen, B. A., Klepeis, J. L., Kolossváry, I., Moraes, M. A., Sacerdoti, F. D. et al. (2006) Scalable algorithms for molecular dynamics simulations on commodity clusters. SC '06 Proceedings of the 2006 ACM/IEEE conference on Supercomputing, Tampa, FL, U.S.A., 11–17 November 2006, Article 84

4 Srebotnik, E., Jensen, K. A. and Hammel, K. E. (1994) Fungal degradation of recalcitrant nonphenolic lignin structures without lignin peroxidase. Proc. Natl. Acad. Sci. U.S.A. **91**, 12794–12797

5 Shary, S., Ralph, S. A. and Hammel, K. E. (2007) New insights into the ligninolytic capability of a wood decay ascomycete. Appl. Environ. Microbiol. **73**, 6691–6694

6 Hammel, K. E., Jensen, K. A., Mozuch, M. D., Landucci, L. L., Tien, M. and Pease, E. A. (1993) Ligninolysis by a purified lignin peroxidase. J. Biol. Chem. **268**, 12274–12281

7 Stoll, S. and Schweiger, A. (2006) EasySpin, a comprehensive software package for spectral simulation and analysis in EPR. J. Magn. Reson. **178**, 42–55

Received 18 February 2013/28 March 2013; accepted 3 April 2013
Published as BJ Immediate Publication 3 April 2013, doi:10.1042/BJ20130251